Two-Photon Absorption in CdSe Colloidal Quantum Dots Compared to Organic Molecules

Nikolay S. Makarov,[†,#] Pick Chung Lau,[§] Christopher Olson,[∞] Kirill A. Velizhanin,[⊥] Kyril M. Solntsev,[†] Khanh Kieu,[§] Svetlana Kilina,[∞] Sergei Tretiak,[‡] Robert A. Norwood,[§] Nasser Peyghambarian,[§] and Joseph W. Perry*[,†]

[†]School of Chemistry and Biochemistry and Center for Organic Photonics and Electronics Georgia Institute of Technology, Atlanta, Georgia 30332, United States, [∞]Department of Chemistry and Biochemistry, North Dakota State University, Fargo, North Dakota 58108, United States, [‡]Theoretical Division, T-1/CINT, and [⊥]Theoretical Division, Los Alamos National Laboratory, Los Alamos, New Mexico 87545, United States, and [§]School of Optics, University of Arizona, Tucson, Arizona 85721, United States. [#]Present address: Currently at Center for Advanced Solar Photophysics, Los Alamos National Laboratory, Los Alamos, New Mexico.

ABSTRACT We discuss fundamental differences in electronic structure as reflected in one- and two-photon absorption spectra of semiconductor quantum dots and organic molecules by performing systematic experimental and theoretical studies of the size-dependent spectra of colloidal quantum dots. Quantum-chemical and effective-mass calculations are used to model the one- and two-photon absorption spectra and compare them with the experimental results. Currently, quantum-chemical calculations are limited to only small-sized quantum dots (nanoclusters) but allow one to study various environmental effects on the optical spectra such as solvation and various surface functionalizations. The effective-mass calculations, on the other hand, are applicable to the larger-sized quantum dots and can, in general, explain the observed trends but are insensitive to solvent and ligand effects. Careful comparison of the experimental and theoretical results allows for quantifying the range of applicability of theoretical methods used in this work. Our study shows that the small clusters can be in principle described in a manner similar to that used for organic molecules. In addition, there are several important factors (quality of passivation, nature of the ligands, and intraband/interband transitions) affecting optical properties of the nanoclusters. The larger-size quantum dots, on the other hand, behave similarly to bulk semiconductors, and can be well described in terms of the effective-mass models.

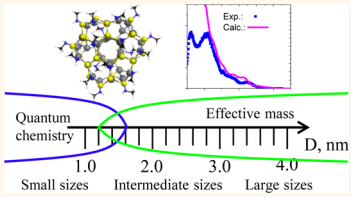

KEYWORDS: quantum dot · CdSe · two-photon absorption · quantum-chemical calculations · effective-mass model

Over the last few decades the use of semiconductor quantum dots (QDs) as optical chromophores has attracted broad research interest in condensed-matter physics and physical chemistry. Owing to quantum confinement effects, synthetic control over the QD size allows for effective tuning of their absorption and emission across a broad spectral range.[1] It is especially advantageous that the same chemical modification methods can be used for variously sized QDs, thus providing chromophores with different colors. Because of their photostability and a variety of possible surface chemical functionalizations, QDs are particularly attractive for biomedical labeling and microscopy.[2,3] Accordingly, the linear optical properties of colloidal QDs have been exhaustively studied both experimentally and theoretically.[4−11] The majority of QD theoretical studies are based on condensed matter approaches. For example, the parabolic band approximation for CdS (or CdSe) QDs[10] considers single conduction and three valence bands and ignores coupling between them. Nonparabolic corrections can be accounted for by including these couplings within, for example, $k\cdot p$ theory,[4] which considers mixing between the heavy- and the light-hole bands, but still ignores mixing of the conduction and valence bands. The eight-band effective-mass model[11] generalizes $k\cdot p$ theory by adding coupling between the conduction and valence bands and considers the complex structure of the valence bands. Usually the more detailed models are the best in quantitative description of transition energies and spectra, but they also lose the advantage of simplicity, physical transparency, and intuitive interpretation. In addition to these condensed matter methods, more recent quantum-chemical electronic structure calculations based on

* Address correspondence to joe.perry@gatech.edu.

Received for review September 24, 2014 and accepted November 26, 2014.

Published online November 26, 2014
10.1021/nn505428x

the density functional theory (DFT) have related electronic structure and dynamics of small QDs to their atomistic composition and surface properties.[12−17]

Compared to QDs, organic conjugated molecules constitute another important class of optically active chromophores, where enhanced nonlinear optical (NLO) polarizabilities suggest a number of technological applications such as bioimaging[18] and 3D microlithography.[19] Numerous studies have been conducted to reveal structure−property relationships for the NLO response of organic molecules[20−23] and fluorescent proteins.[24] This work has benefitted from the development of elaborate quantum-chemical techniques[20,25−28] allowing for predictive calculations of NLO responses in organic molecules and detailed analysis of the underlying electronic properties. Thus, various synthetic approaches have been widely explored to engineer the desired NLO properties of the molecules. For example, variation of the conjugation length[29,30] allows for tuning transition energies and transition strength for both linear and nonlinear absorption. Electron donor/acceptor substituents[20−22,28,31,32] can further modify and enhance optical properties. Finally, branching[26,33,34] is an efficient way of enhancing the NLO response of molecules, whereas it typically has a minor effect on the linear optical spectra.

The availability of the attractive, inexpensive synthetic routes for the QDs combined with their superior NLO properties[4−6] enables them to be potential competitors with organic molecules in the endeavor for NLO applications. Fewer opportunities for modification and NLO enhancement have been explored for QDs, as only limited experimental data are available on their NLO properties.[4−9] Various theoretical approaches[7−11] have been used to interpret these experimental data. These models, however, almost completely ignore the broad quantum chemistry approaches developed for organic molecules.[20,25−27] Additionally, in the majority of studies, the merit of a particular model is determined mainly on the basis of reproducing experimentally observed transition energies. Much less attention has been paid to the agreement between experimental and theoretical values of the respective dipole moments and NLO absorptivities and, therefore, to agreement between experimental and simulated absorption spectra on an absolute scale. Therefore, detailed understanding of the relationship between the structure and chemical composition of QDs and their NLO responses is currently missing. For example, controlling the QD size allows one to tune optical spectra in a way somewhat similar to the variation of the conjugation length in the molecules. However, the effects of shape control and surface chemistry are much less explored, but can also be used to fine-tune optical properties and NLO responses.

Here we present a systematic experimental and theoretical study of the linear and nonlinear optical responses of colloidal QDs focusing on their electronic structure and properties. We extensively use methodologies developed for organic molecules, apply them to QDs, and then compare and contrast the results to those for the organic molecules to highlight both similarities and differences for these two types of nanoscale chromophores, which potentially can be used in the same applications, such as biological fluorescent markers, nonlinear optical limiters, etc. In particular, we measure the one-photon (1PA), two-photon (2PA), and transient absorption (TA) spectra of CdSe core-only and CdSe/ZnSe core/shell QDs with varying core sizes and shells. We further calculate 1PA and 2PA spectra and compare the results with the experimental observations. Specifically, we test whether the NLO response of QDs can be described using a sum-over-states expression with the same calculation techniques as used for organic molecules.[20,25−27] As full quantum-chemical calculations are not feasible for the large-size QDs, containing hundreds and thousands of atoms, we examine the applicability of effective-mass calculations to the description of the NLO response of the larger sized QDs. We also report the theoretical characterization of the linear, and for the first time, two-photon optical properties of the ligated $Cd_{33}Se_{33}$ clusters using time-dependent (TD-) DFT.[25,26] The effects of partial and full surface ligation, as well as the role of solvent, are discussed in terms of the optical oscillator strengths, as well as frequency dependent polarizabilities and hyper-polarizabilities.

Our study allows us to quantify the ranges of applicability of theoretical methods used in this paper with respect to the size of semiconductor nanocrystals. Scheme 1a illustrates three distinct size scales for the QDs identified for the CdSe with a lattice constant of 0.6 nm and an exciton Bohr radius of 5 nm.[35] For large-sized dots (more than ∼3 nm in diameter) the effective-mass approximation is adequate to describe both 1PA and 2PA spectra. Further, the surface states only weakly affect the optical spectra, and the QDs represent a continuous transition toward the bulk. Therefore, solid-state theoretical methods such as comprehensive effective-mass approximations are well suited to quantitative description of these QDs. Small dots (nanoclusters) ∼1.3−1.5 nm in diameter behave somewhat like macro-molecular systems. Consequently, the types of ligands, their surface densities and positions are important to the electronic properties of these chromophores, so that only quantum chemistry techniques can adequately describe their linear and nonlinear optical absorption spectra. Previously QDs of this size-range were not readily available for experiments due to challenging synthetic approaches and low stability. The chemical composition and conformation of these nanoclusters are hard to control as the rigid semiconductor crystal core is not yet fully developed in them. However, this situation is changing rapidly with

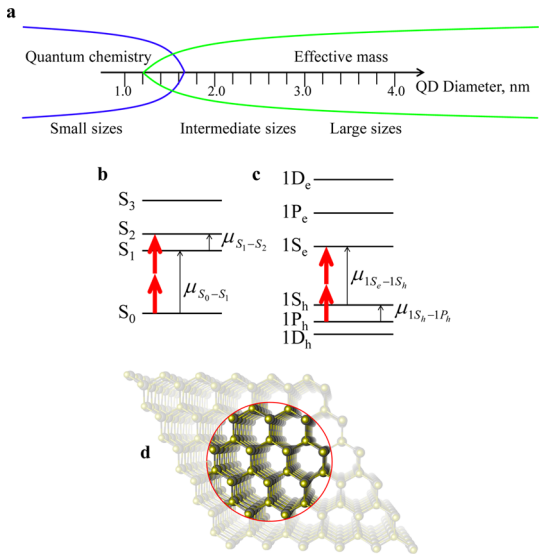

Scheme 1. (a) Three important size regions of QDs can be readily recognized. For QDs with the diameter more than 3 nm (large size), the effective-mass model is adequate in describing both 1PA and 2PA spectra, and the behavior of quantum dots resembles that of a bulk semiconductor. For the smallest dots (nanoclusters), ~1.3-1.5 nm diameter (and smaller), surface states, types of ligands, their number and positions are important, so only quantum chemistry can be used to adequately describe the absorption spectra, and therefore, the nanoclusters can be thought as large macromolecules. In between these two regions, there is an intermediate size window where the effective-mass model becomes inadequate as the size of QDs approaches the size of unit cell of the bulk material, while quantum chemistry is limited due to computational resources. Other approaches, such as multiband effective-mass models, excitonic calculations, pseudopotential methods, or mixed calculations might be appropriate in this size region. In this window confinement effects are important, and therefore quantum dots of these sizes cannot be directly compared to molecules or bulk semiconductors. Comparison of the electronic structure of centrosymmetrical organic molecules (b) and quantum dots (c) highlights important differences and similarities: the strength of the two-photon allowed transitions in centrosymmetrical molecules is defined by dipole moments between the ground (S_0) and excited state (S_i, $i > 0$) and between the two excited states (for example, the S_0-S_2 transition can be mostly determined by the dipole moments between the states S_0 and S_1 ($\mu_{S_0-S_1}$) and S_1 and S_2 ($\mu_{S_1-S_2}$), where excited state S_1 acts as an intermediate virtual level). For QDs, on the other hand, the 2PA strength is determined by the dipole moments of the interband and intraband transitions. For example, the $1S_e \rightarrow 1P_h$ transition is mostly determined by the dipole moments of the $1S_h \rightarrow 1S_e$ interband transition ($\mu_{1S_e-1S_h}$) and $1P_h \rightarrow 1S_h$ intraband transition ($\mu_{1S_h-1P_h}$), where the $1S_h$ state acts as an intermediate level. Therefore, interband dipole moments of QDs can be compared to the dipole moments between the ground and excited states of organic molecules, while intraband dipole moments can be compared to dipole moments between the excited states. (d) Construction of spherical $Cd_{33}Se_{33}$ nanocluster from the wurtzite-type lattice of bulk CdSe

the recent introduction of the stable synthetic routes for such nanoclusters.[36,37] In between these two size ranges there is an intermediate size window, where the electronic properties of QDs are strongly controlled by quantum confinement phenomena. Such QDs represent chemically and optically stable nanostructures, with NLO that can fully benefit from the confinement effects. Unfortunately, in this size regime, effective-mass models become inaccurate because structural atomistic details are important. Likewise, quantum chemistry approaches are not yet tractable due to limitations in computational power available. Other approaches, such as multiband effective-mass models,[4,11] excitonic calculations[7] or pseudopotential methods[38−40] might be appropriate in this size window, though further studies are necessary to test these methods.

Below we compare experimental and theoretical 1PA and 2PA spectra of CdSe QDs for all three size ranges. To facilitate the physical interpretation of the obtained results, the 1PA and 2PA spectra were simulated using a simple single-band effective mass model. Despite known deficiencies (*e.g.*, lack of interband coupling), we find that linear (1PA) and nonlinear (2PA) optical properties of the large-size regime QDs are described rather well by this model. Notably, 1PA and 2PA cross sections are found to be comparable to that of the best organic molecules. The 2PA cross sections at 800−815 nm follow bulk volume scaling similar to that observed for 1PA at 400 nm. In the intermediate-size regime, comparison of the spectra measured experimentally and calculated using the effective-mass model suggests deviation from the trends observed for the larger-sized QDs. The effective-mass models become inaccurate as the optical properties are affected by structural details at the atomic scale. The 2PA volume scaling still holds at 800 nm, but not at 815 nm. For the small nanoclusters, significant deviations between the effective-mass and quantum-chemical calculations suggest that the detailed description of QD surfaces is important for proper determination of their optical properties.

RESULTS AND DISCUSSION

Large-Size Quantum Dots. Electronic properties of semiconductor nanocrystals gradually deviate from their bulk counterparts once the QD dimensions become smaller than the exciton Bohr radius, reflecting quantum confinement effects.[11,41,42] For the large-size regime (see Scheme 1a), band theory and effective-mass models[4,10,11] are well established methods allowing for quantitative description of electronic bands and the resulting optical properties of QDs.

Figure 1 compares experimental 1PA and 2PA spectra of the six differently sized core-only QDs (diameter from 3.1 to 4.5 nm) with the effective-mass calculations. The 1PA spectra show a broad size-dependent transition at ~541−590 nm, and a shoulder at ~503−560 nm, followed by a rapid increase toward shorter wavelengths with two additional shoulders noticeable at ~451−484 nm and ~378−393 nm. Supporting Information (SI), Table SI1 lists the peak wavelengths for the lowest energy transition (λ_{1PA}^{red}) and its

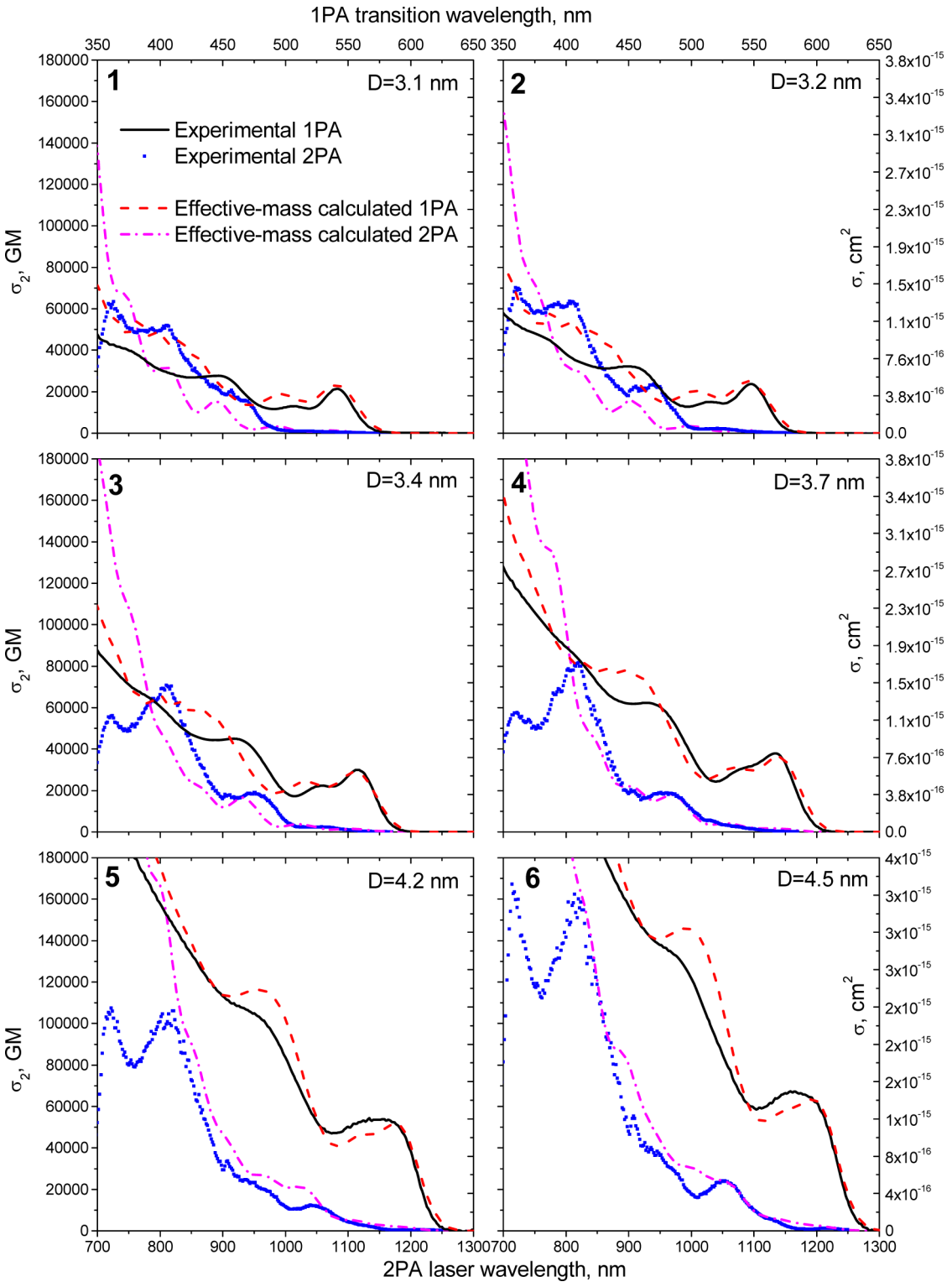

Figure 1. Comparison of the one-photon (black and red lines) and two-photon (blue symbols and magenta lines) absorption spectra of the six large-size QDs in hexane measured experimentally (black and blue) and calculated using the effective-mass model (red and magenta) shows that these QDs can be reasonably well described by bulk-like band models taking into account quantum confinement effects.

maximum cross sections and molar absorptivity (σ_{1PA}^{red} and ε_{1PA}^{red}, see SI for details on measurements). The observed 1PA bands are typically attributed to the $1S_{h_{3/2}} \rightarrow 1S_e$, $2S_{h_{3/2}} \rightarrow 1S_e$, $1P_{h_{3/2}} \rightarrow 1P_e$, and $3S_{h_{1/2}} \rightarrow 1S_e$ transitions, respectively.[11,43] In our effective-mass model we ignore spin–orbit coupling and introduce "soft" selection rules for orbital momentum (see Methods). Henceforth we omit the spin index of the

holes in denoting transitions, as it is not that important in the context of this study. The spectra calculated using the effective-mass model are similar to those measured experimentally, if the calculated energies are empirically corrected according to expression $\bar{\nu} \approx \bar{\nu}_{calc}(1 - 0.06(1 - R/R_0))$. Here, $\bar{\nu}$ are the transition frequencies used to calculate spectra, $\bar{\nu}_{calc}$ are the transition frequencies obtained from the effective-mass model, R is the radius of the QD, and R_0 = 2.50 nm. As the size of QDs decreases, however, our calculations tend to overestimate the absolute values of the molar absorptivity at shorter wavelengths.

Overall, λ_{1PA}^{red}, σ_{1PA}^{red}, and transition dipole moments increase with an increase of the size of QDs. This is similar to the behavior of conjugated organic molecules; those peak wavelengths and cross sections tend to grow with an increase of the conjugation length until saturation is reached.[29,30] Notably, the absorption of QDs shows an almost monotonic increase toward shorter wavelengths. This follows a characteristic behavior observed in the parent bulk semiconductor.[44] In contrast, optical spectra of the common conjugated organic molecules typically have only a few pronounced transitions.[29−34] This increase is attributed to the growth of the density of states further away from the band gap, but not to an increase of the associated transition dipole moments themselves.

2PA spectra have very weak cross sections for the laser wavelength at twice the λ_{1PA}^{red}, supporting the 2PA symmetry dipole-forbidden nature of the lowest energy transition in the QDs. However, the dipole selection rules are partially softened under realistic conditions due to band mixing and nonspherical QD shapes, as discussed in the Methods. This results in the appearance of allowed 2PA excitations in this range due to the $1S_h \rightarrow 1S_e = 1P_h \rightarrow 1S_e + 1P_h \rightarrow 1S_h$ transition as well as the $1S_h \rightarrow 1S_e = 1S_h \rightarrow 1P_e + 1P_e \rightarrow 1S_e$ transition. At shorter wavelengths, the 2PA spectra reveal three peaks (at 1055, 815, and 715 nm for QD **6**) and a shoulder (at 950 nm for QD **6**). The positions of the two high-energy peaks seem to be independent of the QD size, while the lower-energy bands red-shift with an increase in QD size. The spectra reveal a drop in 2PA near 700 nm, which is counterintuitive compared to 1PA. This is, however, consistent with the 2PA of bulk CdSe (see Figure 2 below) and with the results of quantum-chemical calculations for the small nanoclusters (see Figure 5 below). Interestingly, in this spectral range both 1PA and 2PA are overestimated by the effective-mass model, probably suggesting that the high excited-state transition dipole moments are overestimated. A similar issue is known for more sophisticated computational methods, where 2PA sometimes does not converge due to an insufficient number of excited states considered, but is not well studied for the band models. For example, in our case of quantum chemistry calculations of small nanoclusters,

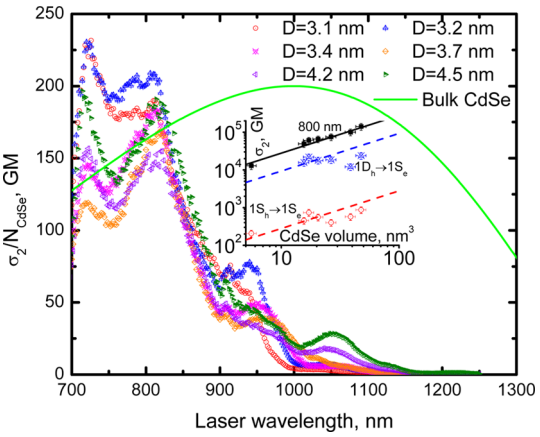

Figure 2. Two-photon absorption spectra of the quantum dots (symbols) normalized by the number of pair of Cd−Se atoms resemble bulk-like behavior at short wavelengths, and show confinement effects at longer wavelengths. The green line shows two-photon absorption of bulk CdSe renormalized per pair of Cd−Se atoms. The inset shows 2PA cross sections at 800 nm (black squares), the $1S_h \rightarrow 1S_e$ transition (red circles), and the $1D_h \rightarrow 1S_e$ transition (blue triangles) as functions of the QDs volume. Black line shows volume scaling for the 800 nm cross sections based on the bulk 2PA. Blue and red lines are guides for the eye to show deviations from linear volume scaling.

only a limited number of states in the low energy portion of the electronic spectrum is computationally accessible, subsequently, the sum-over-states convergence progressively decreases for the high energy spectral window. As we discuss below, in this spectral range QD states are typically considered as bulk-like, and therefore the 2PA should follow that of the bulk CdSe, as observed. Simple effective-mass models, on the other hand, are not well suited for description of the transitions away from the band edge. In addition to this, quantum-interference between transitions with similar strengths is not taken into account by effective-mass models, which can affect calculated 2PA spectra (see the Methods section for more information). This is especially important at high transition energies, where the likelihood of having transitions with similar strength increases because of the high density of states.

Effective-mass calculations suggest that the transitions dominating observed peaks are $1D_h \rightarrow 1S_e = 1P_h \rightarrow 1S_e + 1P_h \rightarrow 1D_h$ for the first peak (*c.f.* transition energy ~18700 cm^{-1} for QD **6**), $1D_h \rightarrow 1D_e = 1F_h \rightarrow 1D_e + 1F_h \rightarrow 1D_h$ for the second peak (*c.f.* transition energy ~23705 cm^{-1} for QD **6**), and $1G_h \rightarrow 1D_e = 1F_h \rightarrow 1D_e + 1F_h \rightarrow 1G_h$ for the third peak (*c.f.* transition energy ~26630 cm^{-1} for QD **6**), while the shoulder roughly coincides with the transition $1F_h \rightarrow 1P_e = 1D_h \rightarrow 1P_e + 1D_h \rightarrow 1F_h$ (*c.f.* transition energy ~22340 cm^{-1} for QD **6**). Calculations also suggest that the transitions $1P_h \rightarrow 1P_e = 1D_h \rightarrow 1P_e + 1D_h \rightarrow 1P_h$ and $1P_h \rightarrow 1P_e = 1P_h \rightarrow 1D_e + 1D_e \rightarrow 1P_e$ (*c.f.* ~19780 cm^{-1} for QD **6**) should be visible in 2PA spectra; however, our experimental results do not confirm this. Overall, the calculated

spectra tend to underestimate the absolute 2PA cross sections in the 800−1000 nm spectral range, especially for the smaller-size QDs, and overestimate it at the shorter wavelengths. The agreement between effective-mass calculations and experimental data is typically better for low-energy transitions and gets progressively worse for the higher-energy transitions.[11] This behavior can be explained by the ligand/surface states strongly affecting high-energy transitions. Indeed, ligand transitions in the UV spectral range mix effectively with the bulk-like states of the QDs (see discussion on the quantum-chemical calculations in what follows). Interestingly, our calculations show that the hole intraband transitions dominate the 2PA response. This can be qualitatively attributed to the larger density of states for the valence band of CdSe QDs. Because of the larger effective masses of holes, the spacing between their states is small, and therefore, the detuning factor $\nu_{im} - \nu$ (see eq 5) is typically smaller for the holes. Thus, the contribution from the holes is larger, and thus 2PA allowed transitions typically involve an intermediate state in the valence band.

An important distinction can be made between QDs and organic molecules based on the comparison of the 1PA and 2PA spectra in Figure 1. For noncentrosymmetric molecules[20,21,27−32] optical selection rules allow the same transitions to be accessible by both 1PA and 2PA processes. The opposite is true when the molecule possesses inversion symmetry,[26,33,34] so that excited states of different symmetry, odd to even, are allowed for 1PA, but even to even are allowed for 2PA excitations, respectively. In the case of the QDs, on the other hand, selection rules require a change of orbital momentum of $\Delta L = 1$ for the intraband transitions, which generally places the 2PA transition energies close to the 1PA transition energies, as the hole states are densely spaced. This produces a slight blue shift for the 2PA peaks when compared to their 1PA counterparts. To make a few specific comparisons between QDs and centrosymmetric conjugated molecules of similar size, we consider the 1PA and 2PA properties of a so-called extended squaraine molecule, see dye **3** from ref 45, that has a molecular length of ∼3.6 nm. The 1PA molar absorptivity of dye **3** is 3.5×10^5 M^{-1} cm^{-1} at 856 nm ($\sigma \approx 1.3 \times 10^{-15}$ cm^2), in comparison to the 3.4 and 3.7 nm CdSe QDs, which have molar absorptivities for the lowest exciton band of 1.7×10^5 M^{-1} cm^{-1} at 557 nm ($\sigma \approx 6.4 \times 10^{-16}$ cm^2) and 2.1×10^5 M^{-1} cm^{-1} at 567 nm ($\sigma \approx 8.1 \times 10^{-15}$ cm^2). The absorption is lower than but comparable to that of the extended squaraine dye **3**. The 2PA cross section of the squaraine dye **3** is 33 000 GM at 1050 nm, which is again rather close in magnitude to those of the 3.4 and 3.7 nm QDs. The 3.4 and 3.7 nm QDs both exhibit 2PA cross sections of ∼18 000 and 19 000 GM at ∼960 nm, fairly close to the value for squaraine dye **3**. In both cases, the 2PA active transition does not correspond to the lowest-energy 1PA transition, but does overlap with one of the higher-energy transitions.

Overall, the 2PA cross sections of our QDs are similar to those reported in ref 4. The cross sections increase with increasing QD size, and the concomitant red-shifts of the confined low-energy bands suggest similarities to the delocalized transitions of the organic molecules, while the bulk-like higher-energy transitions, which do not shift much with the size, are similar to the spatially localized transitions of organic molecules.

As we argued above, the optical properties of large-size QDs are expected to show similarities to those of bulk semiconductors. In this regard, it is interesting to compare 2PA of the QDs with that of bulk CdSe.[46] The peak QD cross sections at 800−815 nm have values very close to the product of the peak cross section of bulk CdSe and the number of atom pairs in the QD. This is illustrated in Figure 2, which shows 2PA spectra of QDs normalized to the number of CdSe atom pairs overlapped with the 2PA of bulk CdSe. This suggests that 2PA at short wavelengths (∼700−800 nm) is dominated by bulk effects, while the longer-wavelength absorption is due to confinement effects and is less than that of a bulk crystal. Consequently, the 2PA peaks at ∼720 nm and ∼810 nm do not shift with the QD size, while the position of the longer-wavelengths peaks is strongly affected by the QD size. A similar trend is well-known for the linear absorption, where cross sections of QDs are often compared to the bulk based on volume scaling[47] at high energies (typically 3.1 eV), where the energy levels are considered to be bulk-like. Interestingly, Figure 2 suggests that all QDs of this size range have a 2PA transition band at ∼1050 nm, where strength progressively decreases as the size of QDs decreases. One should keep in mind, however, that all the transition energies shift with QD size, and, therefore, this peak corresponds to different transitions for the different QDs, from $1S_h \rightarrow 1S_e$ = $1P_h \rightarrow 1S_e + 1P_h \rightarrow 1S_h$ for the QD **1** to $1D_h \rightarrow 1S_e$ = $1P_h \rightarrow 1S_e + 1P_h \rightarrow 1D_h$ for the QD **6**.

The inset to Figure 2 shows more specifically that the linear volume scaling of the 2PA cross sections is valid at 800 nm (black symbols and black line), while the quantum confinement affects lower-energy transitions, such that their volume scaling deviates from the linear (blue and red symbols, note that the cross sections of the 4.5 nm QDs are almost the same as for the 3.2 nm QDs for the $1S_h \rightarrow 1S_e$ and $1D_h \rightarrow 1S_e$ transitions).

To validate our expectation that the 1PA and 2PA of the large-size QDs are not that sensitive to passivation and ligand effects, we have performed measurements of core/shell QDs (see SI, Figures SI5 and SI6 for details). The spectra are only slightly affected by the presence of the shell at short wavelengths due to absorption of the shell material. More sophisticated shell architectures,

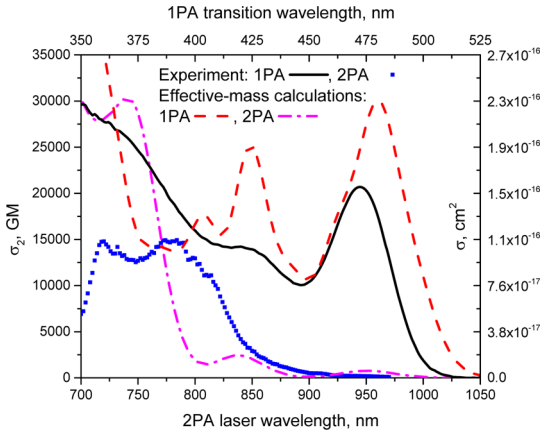

Figure 3. Comparison of the one-photon (black and red lines) and two-photon (blue symbols and magenta lines) absorption spectra of the $Cd_{111}Se_{111}$ QD in hexane measured experimentally (black and blue) and calculated using the effective-mass model (red and magenta) shows disagreement in the position and intensity of the transition bands, suggesting that the QDs of this size behave more like quantum confined nanostructures, which require special techniques to be used for their accurate theoretical description.

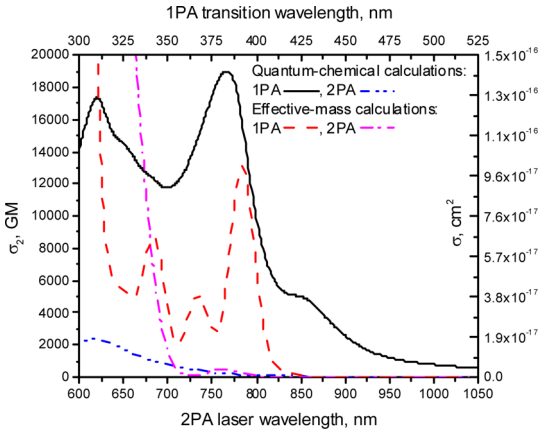

Figure 4. Comparison of the one-photon (black and red lines) and two-photon (blue and magenta lines) absorption spectra of the $Cd_{33}Se_{33}$ QD calculated using quantum-chemistry approach (black and blue) and effective-mass model (red and magenta) shows significant differences in lineshapes and transition strengths, suggesting that for this size of QDs, the effective-mass approach can be used only for a qualitative description of the optical spectra.

however, are available for "engineering" of wave functions and controlling QD properties; use of such core/shells structures, mostly not yet tested, can result in significant improvements of the NLO properties.[48]

Intermediate-Size Quantum Dots. As the size of QDs is further decreased, it approaches the extent of the bulk semiconductor unit cell. In this case, the effective-mass approach is expected to fail.[11] As is evident from the smallest size of QDs in Figure 1, this trend is indeed well observed. To study QDs in this intermediate size range we synthesized a larger cluster with ~2.2 nm diameter. This size roughly corresponds to a $Cd_{111}Se_{111}$ structure, which may be constructed by adding an extra atom-thick layer on the top of the smaller $Cd_{33}Se_{33}$ cluster.

Figure 3 compares 1PA and 2PA spectra of the $Cd_{111}Se_{111}$ QDs measured experimentally and calculated using the effective-mass model. As expected, contrary to the larger-size QDs, effective-mass calculations show much greater disagreement with the experiment for both 1PA and 2PA spectra. The calculated 1PA peaks are red-shifted, narrower and stronger compared to those observed experimentally. This can be partially explained by a somewhat broader size distribution and the possible errors in size determination of the synthesized QDs, which would be hard to estimate due to the limited resolution of the TEM images. Calculated 2PA cross sections are smaller compared to the experimental data for the 800–900 nm spectral range; however, the situation is reversed at the shorter wavelengths. Notably, calculations qualitatively preserve the 2PA spectral features, which can be compared to the typical uncertainties encountered when contrasting the experimental and calculated spectra of organic molecules.[26] The calculated transitions appear to be blue-shifted compared to the experimental data, and the observed trends suggest that QDs of this size behave more like quantum confined nanostructures, which requires special techniques to be used for their accurate theoretical description. Even though the eight-band model[11] might be partially useful here, it still has the limitations of all the effective-mass models as atomistic features become important for this size-range of QDs; accordingly more sophisticated numerical approaches are desired. Quantum chemistry can potentially become applicable as computation power improves and better algorithms are developed. At the moment, however, excitonic calculations[7] or pseudopotential methods[38–40] seem to be the most appropriate candidates for theoretical description of the optical properties of QDs in this size range.

Notably, bulk volume scaling for the 2PA cross sections at 815 nm (see above) does not apply for this size of QDs, and the experimental value is almost 40% lower than that of the bulk. At wavelengths shorter than 780–800 nm, though, the 2PA cross sections of the QDs closely follow the bulk CdSe value. This suggests that as the QD size decreases, higher-energy states can be considered as bulk-like states, while the states below ~3 eV are altered by quantum confinement effects.

Even though it is expected that the nanostructures in this size window should fully benefit from the quantum confinement effect, our measurements show that this does not improve their NLO properties. Instead, 2PA gets reduced (compared to the bulk volume scaling), suggesting that surface effects are detrimental to the NLO properties. This is further supported by the following discussion.

Nanoclusters. As the size of the QDs is decreased even further, the effects of individual atoms, surfaces, and ligands on the optical responses become even

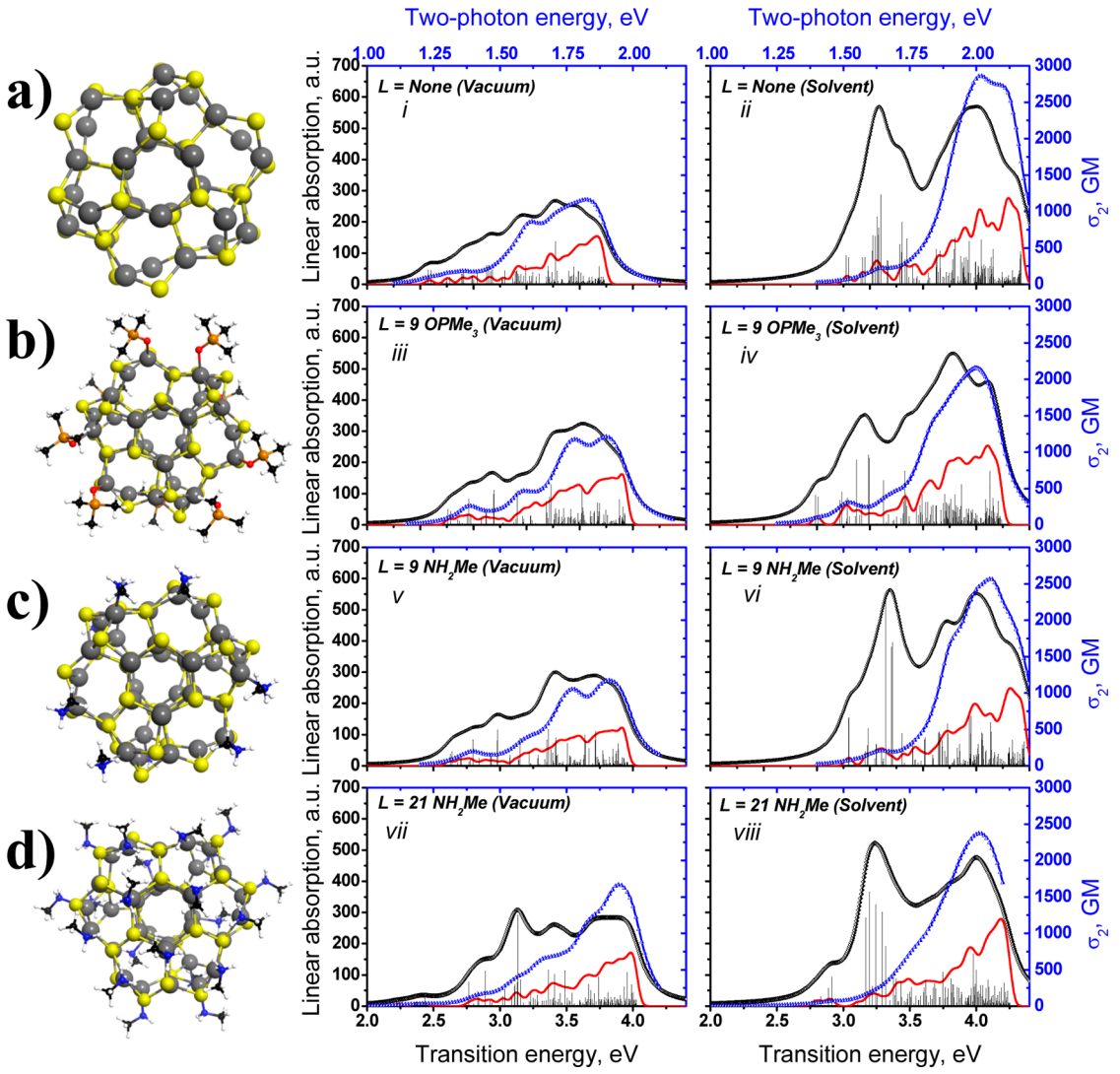

Figure 5. One- (black lines) and two-photon (blue lines) absorption spectra of the $Cd_{33}Se_{33}$ QDs calculated using the quantum-chemical approach show the importance of solvent environment and ligands effects. Panels a, b, c, and d correspond to an unpassivated cluster, and passivated with 9 $OPMe_3$, 9 NH_2Me, and 21 NH_2Me model systems, respectively. Vertical dark gray lines correspond to the oscillator strength of optical transitions. The red line shows the density of excited states, which includes all possible transitions. The 1PA and 2PA energies are scaled accordingly (to transition energies) to highlight the similarities or differences between the spectra.

more important. Unfortunately, these small-sized QDs, often termed nanoclusters,[49,50] are not readily available for experimental measurements. We, therefore, restrict our discussion here to comparison of their optical spectra calculated using effective-mass and quantum-chemical methods only.

Figure 4 shows that effective-mass and quantum-chemical calculations of the $Cd_{33}Se_{33}$ spectra only agree qualitatively with each other. The narrow absorption peak previously experimentally observed in $Cd_{33}Se_{33}$ at 389 nm[49,50] is in between the calculated values (383 nm for quantum-chemical and 392 nm for effective-mass calculations). The shoulder (~425 nm) seen in quantum-chemical calculations is typically ascribed to larger-size QDs, but in our case it is due to ligand-localized states. While effective-mass calculations are mostly not applicable in the case of nanoclusters, and can give only qualitative information about their optical properties, quantum-chemical calculations are efficient for these sizes, and can address various questions, including the quality of the ligand passivation and solvent effects. Comparison of both 1PA and 2PA to the volume scaling shows that the estimated 1PA cross sections (11.5×10^{-17} cm^2 at 400 nm) is somewhat larger than that given by quantum-chemical calculations (7.6×10^{-17} cm^2) or effective-mass calculations (5.0×10^{-17} cm^2). The 2PA volume scaling does not hold at any wavelength for this size of QDs, showing once again the importance of surface and ligand states.

Figure 5 illustrates the importance of the ligand states by comparing spectra calculated for unpassivated and passivated clusters (panels a–d). In the case of bare and partially passivated QDs in vacuum, the

2PA and 1PA spectra closely follow each other. With the unpassivated dot as a benchmark, a slight blueshift in the first maxima of 2PA occurs upon ligation with NH_2Me and $OPMe_3$. It is interesting to note that the chemical nature of the binding ligand (*via* oxygen or nitrogen) seems to have little effect on the characteristics of the 2PA (compare Figure 5, plots *iii* and *v*), and only a minor reversal of high-energy intensity in the region of 3.5−3.8 eV is noted for the 1PA. Overall, the ligand addition intensifies the lowest-energy transitions (characterized by participating hole states near the top of the valence band and a lowest unoccupied molecluar orbital (LUMO) electron state in the conduction band) in the 1PA in the region of ∼2.6−2.8 eV. This effect is clearly demonstrated for the fully passivated QD (see Figure 5d-*viii*), with a strong enhancement of absorption in the 3.2 eV range (see Figure 5, plots *v* and *viii*). This may be attributed to increased delocalization of participating electron and hole states due to dense ligand coverage effectively providing a large dielectric constant environment outside of the QD. This leads to enhanced overlap of the respective wave functions and thus amplifying the resulting transition dipole moment.

Interestingly, partial and full passivations have opposite effects on the low-energy 2PA. Compared with the bare QD, 2PA of the partially passivated QDs is enhanced below ∼3.0 eV concomitant with the rise in total transition density. Upon full passivation, a strong suppression of 2PA is observed below ∼2.6 eV, whereupon the response increases monotonically with increasing energy (see Figure 5, plot *vii*). Notably, the addition of 9 or 21 ligands enhances the transition-dipole strengths of the low energy transitions, and also enhances the 2PA cross sections for higher-energy transitions as evidenced by the increased magnitude in the ∼1.7−2.0 eV 2PA energy range (plots $i \leq iii \approx v < vii$).

As can be seen in Figure 5, plots *i* and *ii*, the addition of solvent mimics the effect of total passivation of the bare dot, with significant enhancement of both 1PA and 2PA responses resulting from strengthening the low-energy transition dipole moments (compare Figure 5, plots *ii*, *vii*). In agreement with previous results[51] the presence of solvent leads to a blueshift of all optical spectra, although the overall effects are strongest in those structures that are less sterically screened to the dielectric environment by the coordinating ligands (Figure 5a,c). Figure 5, plot *vii* displays the best agreement with experimental results for the smallest measured dots, with the onset of 1PA occurring around 2.2 eV (∼550 nm) and 2PA at 1.2 eV (∼1000 nm). The 1PA demonstrates the previously obtained experimental features up to ∼3.5 eV.[49,50]

Overall, the small size QDs can be, in principle, compared to large size macromolecules, for which quantum-chemical calculations find broad use. Similar to the effects of the conjugation length,[29,30] donor/acceptor substituents,[20−22,31,32] and branching[26,33,34] on the optical properties of organic molecules, the type of ligands and ligand surface density can substantially affect the optical properties of small QDs.

CONCLUSIONS

Significant breakthroughs in understanding structure−property relationships for organic molecules have opened up wide possibilities for their applications, through our ability to fine-tune their linear and nonlinear optical response through structure. However, their relatively low photostability, complicated synthetic chemistry, and also relatively low two-photon cross sections, relative to the larger sized CdSe QDs, pose significant challenges for the wide commercialization of these materials. Semiconductor quantum dots can be considered to be promising candidates to address these weaknesses of organic molecules.

Here, we have performed a systematic study of the nonlinear optical properties of CdSe colloidal quantum dots. We measured two-photon and transient absorption spectra and cross sections of core-only and core/shell quantum dots of various sizes and compared the experimental results with theoretical predictions based on quantum-chemical calculations and the effective-mass model. This allowed us to quantify the ranges of applicability of these simulation techniques.

Comparison of the experimental results with the effective-mass calculations reveals very good agreement for QDs of size larger than 3 nm in diameter, which progressively becomes worse as the size decreases. We believe that this is a very important conclusion since it allows one to use the simple and physically transparent computation methods to gain an insight into complex optical nonlinear processes. Smaller-sized dots require more sophisticated calculation techniques as they resemble nanostructures and nanoclusters where confinement and surface effects play an important role in determining optical spectra. For the smallest $Cd_{33}Se_{33}$ nanoclusters, results of the effective-mass and quantum-chemical calculations agree only qualitatively. Quantum-chemical calculations suggest that the nonlinear optical response of small nanoclusters depends on the level of their passivation, though not strongly on the chemical nature of the binding ligand itself. The inclusion of a dielectric environment intensifies the overall optical response, in addition to a large enhancement of low-lying transitions in the linear absorption.

Our study shows that despite the quantum confinement effects, two-photon absorption of quantum dots is mostly suppressed compared to that of bulk semiconductor. While the two-photon absorption cross sections are among the largest observed to date for a single material structure, they suffer compared to organic molecules due to the large volume and molecular weight of the QDs as well as significant dielectric screening. In general, QDs seem to be similar to quadrupolar and octupolar organic molecules in the

sense that their individual 2PA transitions are well described with pure 3-level systems, however, they are at the same time different from organic molecules in the sense that they have an almost continuous density of states, and therefore calculations of their absorption spectra require consideration of a rather large number of excited states.

Overall, while the 2PA cross sections of QDs are relatively large compared to most organic molecules, they should not be compared directly. First, dielectric screening reduces the effective 2PA cross sections of QDs by almost 1 order of magnitude. Second, for most practical applications, 2PA cross sections normalized by molecular weight (or size) should be considered. The ratio $\sigma_2^{(max)}$/M.W. is the largest for the small QDs, reaching 1 GM/Da. The same ratio for organic molecules can reach much larger values, up to 20 GM/Da[52−54] and above. Finally, even though stability of QDs under light excitation is somewhat better compared to molecules, their stability under ambient conditions (*e.g.*, long-term storage) may be worse due to, for example, oxygen-sensitivity. With respect to applications, the large 2PA cross sections of semiconductor nanocrystals can be attractive for techniques such as single-particle (bio)imaging. Likewise, the broadband spectra of the QDs with their large density of states can be advantageous for other applications, such as optical power limiting.

METHODS

Synthesis of Quantum Dots. CdSe QDs were synthesized as described in ref 55: trioctylphosphine oxide (TOPO; 4.0 g), hexadecylamine (HAD; 2.5 g), and tetradecylphosphonic acid (TDPA; 0.075 g) were mixed into a 50 mL three-neck flask. The solution was repeatedly degassed and purged with argon at 100 °C for 1 h using a Schlenk line. A 1.0 mL aliquot of 1.0 M trioctylphosphine-Se (TOP-Se) precursor solution was then injected into the flask. The reactants were then heated to 280 °C under argon. At this moment, 1.5 mL of cadmium precursor solution was swiftly injected into the reactants. The temperature of the flask dropped by approximately 15 °C. While the temperature was maintained at 265 °C, in order to control the average size of the CdSe QDs, the extractions were performed at minute 1, 3, 9, 11, 13, and 15. In the text we refer to these QD samples as **1** through **6**, respectively.

Unreacted cadmium precursors were separated from QDs by adding an equal volume of methanol (used as an extraction solvent). The resulting mixture was centrifuged at 5000 rpm to obtain the precipitate. The precipitate was then suspended in hexane. This purification process was repeated two times in order to completely remove any trace of unreacted cadmium precursors.

Figure SI1 shows transmission electron microscopy (TEM) images of the synthesized QDs (the images received noise reduction and contrast enhancement for better clarity). The distribution of sizes determined from TEM measurements of QDs is shown in Figure 6, and the average sizes are listed in Supporting Information, Table S1. Each sample shows a predominant size distribution with the variations not more than 8%. At least 300 quantum dots of each sample were used to analyze their size distribution.

Measurement Procedures. 1PA spectra of the QDs in hexane solution were measured using Shimadzu UV-3101PC and PerkinElmer Lambda 15 scanning spectrometers at room temperature. Emission was recorded using J&M TIDAS and Jobin Yvon SPEX Fluorolog-3 spectrofluorimeters. Emission lifetimes were measured using an Edinburgh Instruments time-correlated single photon counting (TCSPC) system. The picosecond excitation pulsed diode laser (LDH-P-C-470, Picoquant) emitting at 467 nm was used as an excitation light source with a

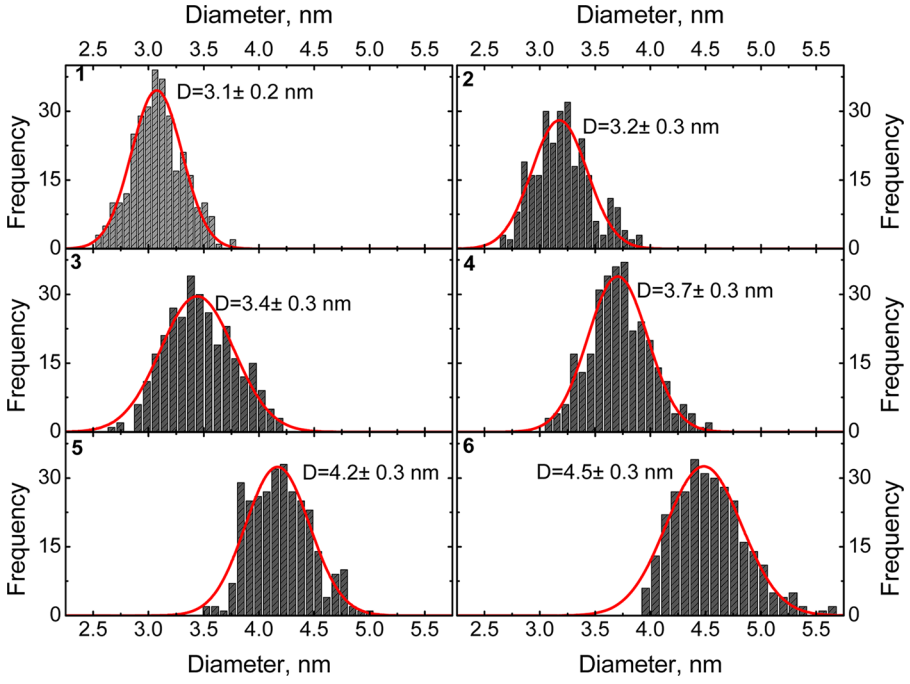

Figure 6. Size distributions of the synthesized CdSe quantum dots.

repetition rate of 200 kHz and a pulse duration of ~140 ps (fwhm). A high-speed microchannel plate photomultiplier tube (Hamamatsu R3809U-50) cooled to −20 °C was used for time-resolved detection. The measurements were done using 50 and 500 ns time windows and 2048 channels with resolutions of ~24 ps/channel and 240 ps/channel, respectively.

TA was measured using an Ultrafast Systems Helios nonlinear spectrometer as described earlier.[56] The excited-state molar absorptivities and cross sections were estimated based on comparison of the TA bleach signal to the 1PA molar absorptivities,[57] together with the measured excited state absorbance and the excited state population distribution along the beam path through the cell.[56]

2PA was measured using a two-arm two-photon excited fluorescence spectrometer as described elsewhere.[58] The spectra were referenced using Lucifer Yellow (λ < 900 nm), Rhodamine 6G (900 ≤ λ ≤ 1120 nm), and Rhodamine B (λ > 1120 nm).[59] The cross sections were measured relative to Rhodamine 6G at λ = 834 nm and λ = 886 nm using 1PA and 2PA excitation of the same samples (concentrations ~1×10^{-6} M, 1 mm path length) in the identical geometry of the same experimental setup. The cross sections of the small QDs were measured relative to Coumarin 485 at λ = 778 nm. To do those measurements one needs to know the 1PA molar absorptivities or cross section as well as emission quantum yields. Detailed descriptions of these measurements and their discussion are given in the SI.

Effective-Mass and Sum-Over-States Calculations. 1PA and 2PA spectra of the larger-sized QDs have been studied theoretically using the effective-mass model.[4,10] This approach allows one to find the QD electronic structure (*e.g.*, transition energies) and its dependence on the dimensions for the QDs by solving the Schrödinger equation for each carrier, that is, separately for electrons and holes, assuming spherical symmetry of the QD. Specifically, the energy of a carrier in a QD was found as an eigenenergy of the following equation for the radial wave function, Ψ_{nL}:[60]

$$-\frac{\hbar}{2}\frac{\mathrm{d}}{\mathrm{d}r}\left(\frac{1}{m(r)}\frac{\mathrm{d}\Psi_{nL}}{\mathrm{d}r}\right)+V(r)\Psi_{nL}+\frac{\hbar^2 L(L+1)}{2m(r)r^2}\Psi_{nL} = E_{nL}\Psi_{nL} \quad (1)$$

where $m(r)$ is the carrier effective mass, L = 0(*S*),1(*P*),2(*D*),··· is the orbital momentum, and n is the radial quantum number, enumerating solutions of the Schrödinger equation for given L, starting from the lowest energy. This equation is solved independently for electrons and holes separately, assuming negative effective mass in the latter case; the exciton energy is then calculated as a sum of the resulting electron and hole energies. The adopted boundary conditions require wave functions to vanish at the surface of the QDs.

The numerical solution of the radial Schrödinger equation is implemented *via* discretization of the radial coordinate, and, therefore, transformation of the Schrödinger differential equation into a matrix eigenvalue problem. We have found that this approach is fast and free of any numerical instability issues. Furthermore, solving the radial Schrödinger equation by transforming it to the matrix eigenvalue problem introduces the possibility of straightforward generalization of the problem for different spherical symmetry core/shell QDs. For example, the continuous variation of effective mass and conduction (valence) band potential (*i.e.*, alloying) is straightforward to implement. This generalization has not been pursued in this paper but will be of great help for future studies.

As a result, atomic-like states defined by the principal quantum number n and orbital angular momentum (S, P, D, ...) are computed for electrons and holes. Using calculated transition energies and wave functions, dipole moments can be obtained in order to compute the 1PA and 2PA spectra using the sum-overstates (SOS) expressions.[61] SOS expressions are used extensively for molecular systems with optical transitions defined by global many-electron states as illustrated in Scheme 1b. Subsequently, calculating the NLO responses involves a summation over the Liouville pathways involving intermediate states coupled by the respective permanent and transition dipole moments. In the case of the effective-mass calculations, electronic transitions are defined as transitions between single-particle electron and hole states (Scheme 1c). This evidences several distinctions of which to take note. First, 2PA transitions in molecules include one ground-to-excited state and one excited-to-higher-excited state dipole moments (Scheme 1b). The corresponding dipole moments for QDs involve one interband and one intraband transitions (Scheme 1c). Second, as the detuning factor ($\nu_{im} - \nu$) becomes large for the intermediate excited states far from the final state, the 2PA response of many molecules with low excited state density can be well described using simplified two- and three-level models, whereas the high density of states in QDs necessitates summation over the all respective inter- and intraband states to obtain converged values of nonlinear optical coefficients. Third, the intraband dipole moments in QDs include both conduction and valence band components, and thus the summation should include both bands. Because of the larger density of states for the valence band of CdSe QDs, however, the detuning factor is typically smaller for the holes, and thus, 2PA allowed transitions typically involve intermediate states in the valence band (see the discussion section).

In our model, the transition dipole moments for the interband transitions are calculated as

$$\mu_i = \mu_{cv}\delta_{\mathrm{Lh,\,Le}}\delta_{\mathrm{mh,\,me}}\int R_h(r)R_e(r)r^2\,\mathrm{d}r \quad (2)$$

where μ_{cv} is the bulk transition dipole moment between the conduction and valence bands, $R_h(r)$ and $R_e(r)$ are the radial wave functions of the hole and electron for the ith transition (with the hole and electron orbital momenta and their projections Lh, Le, mh, and me, respectively) calculated using eq 1. Kronecker delta-symbol $\delta_{\mathrm{Lh,Le}}$ in eq 2 encodes the orbital momentum conservation associated with the interband transition. In a realistic situation, this selection rule becomes less strict due to the nonspherical shape of QDs and the presence of band mixing. The former factor is especially important since once the spherical symmetry of the QD is broken, the parity and orbital momentum of the envelope function are thus not "good" quantum numbers resulting in a nonvanishing mixing between, for example, 1Se and 1Pe. We empirically found that the substitution of $\delta_{\mathrm{Lh,Le}}$ with the "softer" function 1/|Lh − Le|! (exclamation mark stands for the factorial) produces a reasonable agreement between experimental and theoretical (effective mass) results for the 1PA spectrum. This softened selection rule without any further modifications was also used to simulate the 2PA spectrum.

For the intraband transitions, the z-projections of the transition dipole moments are calculated as

$$\mu_j = \sqrt{(2L_i+1)(2L_f+1)}\begin{pmatrix} L_f & 1 & L_i \\ 0 & 0 & 0 \end{pmatrix}\begin{pmatrix} L_f & 1 & L_i \\ -m_f & 0 & m_i \end{pmatrix}\int R_i(r)R_f(r)r^3\,\mathrm{d}r \quad (3)$$

where $R_i(r)$ and $R_f(r)$ are the radial wave functions of the initial and final state (for the electron or hole intraband transition), L_i, and L_f are the orbital momenta of initial and final states, m_i, and m_f are the projections of orbital momentum of initial and final states, and $\begin{pmatrix} L_1 & L_2 & L_3 \\ m_1 & m_2 & m_3 \end{pmatrix}$ are the Wigner 3j symbols. The same approach is used to calculate other projections.

It is well-known that the transition energies calculated using the effective-mass approach deviate from experimental observations.[62] To correct for this discrepancy, we phenomenologcally recalculate the transition frequencies as $\bar{\nu} \approx \bar{\nu}_{\mathrm{calc}}(1 - 0.06(1 - R/R_0))$, where $\bar{\nu}$ are the transition frequencies used to calculate spectra, $\bar{\nu}_{\mathrm{calc}}$ are the transition frequencies calculated from the effective-mass model, R is the radius of the QD, and R_0 = 2.50 nm. This also introduces corrections to the calculated dipole moments.

The calculated interband and intraband dipole moments can typically be directly compared to the experimental 1PA and TA molar absorptivity[21] as

$$|\vec{\mu_i}|^2 g(\bar{\nu}_i) = \frac{3\cdot 10^3\ \ln 10 hc\varepsilon(\bar{\nu}_i)n_0}{(2\pi)^3 N_A \bar{\nu}_i f^2}$$

where N_A is Avogadro's number, h is the Planck constant, c is the speed of light, n_0 is the solvent refractive index, $\bar{\nu}_i$ is the ith transition frequency (in wavenumbers), $g_i(\bar{\nu})$ is the normalized line shape of the ith transition (defined by natural line width and size distribution of the QDs, $\int g_i(\bar{\nu})d\bar{\nu} = 1$), f is the local field factor, and $\varepsilon(\bar{\nu}_i)$ stands for the corresponding band of 1PA molar absorptivity (for the interband transition) or TA molar absorptivity (for the intraband transition) spectra. Unfortunately, because of the large density of states for QDs, such a direct comparison is somewhat complicated, and it is more sensible to calculate the entire spectrum and then compare it to the experimental data (see SI for details). It is important to note that while Lorentz and Onsager field factors are typically used for organic molecules,[21] significant dielectric screening in QDs requires use of the Maxwell-Garnet local field factor.[4]

To obtain absorption spectra we use a sum-over-states expression:[21]

$$\sigma(\bar{\nu}) = \frac{(2\pi)^3 f^2}{3hcn_0} \sum_i \bar{\nu}_i \mu_i^2 g_i(\bar{\nu}) \quad (4)$$

where $\bar{\nu}$ is the frequency, μ_i is the interband transition dipole moment, and the summation is done over all the interband transitions involved.

Similarly, the two-photon absorption (2PA) spectrum can be calculated as[4,21,63]

$$\sigma_2^{(i\rightarrow j)}(\nu) = 2\frac{(2\pi f)^4 \nu^2}{(nhc)^2} \left\langle \left| \sum_m \frac{(\vec{\mu}_{im}\cdot\vec{e})(\vec{\mu}_{mj}\cdot\vec{e})}{(\nu_{im} - \nu)} \right|^2 \right\rangle_{\vec{\Omega}} g_j(2\nu) \quad (5)$$

where $\vec{\mu}_{im}$ and $\vec{\mu}_{mj}$ are the intraband and intraband transition dipole moment, $\vec{e}$ is the unit vector parallel to the optical electric field ($\vec{E} = \vec{e}E$), the summation is performed over all the interband and intraband transitions involved labeled m, and $\langle\rangle_{\vec{\Omega}}$ represents isotropic averaging over all possible orientations of the molecules relative to the excitation optical electric field.

Given that the QDs have intrinsic size dispersion (see Figure 6), to model the actual spectral shapes we calculate 1PA and 2PA spectra not for any specific size, but as a convolution of the eqs 4 and 5 with the QD size distribution. Careful examination of the eq 5 shows that when summation is done over several transitions with relatively equal strengths, quantum interference between these transitions is possible. While such interference can be easily accounted for by quantum-chemical calculations, our effective-mass model does not provide any information on the nature (constructive/destructive) of the interference. Here we assume constructive interference for our 2PA calculations. While it seems to work well for the 2PA wavelengths longer than 800 nm, our model does not describe experimental data well at shorter wavelengths. This might be because destructive interference between transitions (or no interference) starts playing a role at shorter wavelengths.

In our discussion we refer to 2PA transitions in QDs by indicating the states involved and leading dipole moments determining the transition strength. Thus, for example, a 2PA transition between the 1S-electron and 1S-hole states with a 1P-hole intermediate state proceeding according to a 1S-electron to 1P-hole virtual transition plus a 1P-hole to 1S-hole virtual transition is denoted as $1S_h \rightarrow 1S_e = 1P_h \rightarrow 1S_e + 1P_h \rightarrow 1S_h$.

Quantum-Chemical Calculation Techniques. The absorption spectra of the small $Cd_{33}Se_{33}$ nanoclusters have been also calculated using a quantum-chemical approach based on adiabatic time-dependent DFT (TD-DFT)[17] in the Kohn–Sham (KS) form, which is currently the method of choice for calculating the excited-state structure of large molecular systems. TD-DFT extensions for the calculations of molecular nonlinear optical properties have been suggested based on the quasi-particle formalism of the TD-KS equations for arbitrary frequency-dependent nonlinear optical polarizabilities.[25,64] Briefly, this approach calculates the first- and third-order frequency-dependent polarizability tensors using SOS expressions similar to those discussed in the previous section. The inputs are excitation energies, the respective permanent/transition dipole moments, as well as other quantities obtained from TD-DFT simulations. Notably, interpretation of the NLO response computed using the TD-DFT approach *via* global many-body states (Scheme 1b) is intuitively straightforward.[25,65] A detailed description of the method has been reported elsewhere.[25,64] This approach was successfully applied to calculate the 1PA and 2PA properties of several families of donor/acceptor substituted conjugated organic dyes and branched structures.[26,64,66,67] Excellent quantitative performance of TD-DFT based on hybrid functionals has been shown for both 1PA and 2PA responses.

Other sophisticated models have also been used in literature to calculate optical properties of the QDs by separately modeling atoms in the bulk of the QDs *via* semiempirical tight-binding[68,69] and pseudopotential[38,39,70,71] approaches, while modeling the surface passivating molecules through either single oxygen atoms[68] or simplified model potentials.[72] Any realistic model, however, has to explicitly describe bonding between the QD and the ligands, which is lacking or incomplete in the semiempirical pseudopotential-based approaches. Several attempts have been made to model ligated CdSe QDs using force field,[73,74] Monte Carlo,[75] and coarse grained[76] methods. These methods, however, are based on a model description of the molecular framework and interactions. Such parameters are unavailable from measurements, making the justification of these approaches questionable. To overcome this problem, the model parameters are typically derived from first-principle calculations of small clusters of a few atoms in size.

Computational modeling based on TD-DFT has already been shown as a reliable tool in studies of optical properties of small size (<2 nm) QDs with the main focus on the effect of various passivating ligands[77−80] on radiative[13,16] and nonradiative[12,14] photoexcited processes in CdSe QDs. More accurate many-body methods have also been used in studies of optical properties of various small QDs, including coupled cluster,[81] configuration interaction,[82] and multiconfigurational self-consistent field[83] methods. Being reasonably accurate in inclusion of electron−electron and electron−hole correlations, these methods, unfortunately, are computationally demanding and cannot be yet applied to the QD systems containing more than 50 atoms, especially when most of these atoms are transition metals and heavy elements such as Cd. Therefore, TD-DFT remains one of the most common approaches that provide reasonably accurate descriptions of optical properties of 1−1.5 nm QDs, while using moderate computational resources.[84,85]

In this study, we apply TD-DFT methodology[25,64] to model 1PA and 2PA spectra of $Cd_{33}Se_{33}$ clusters with and without ligands. The initial quantum dot geometry is generated through a quasi-spherical cut from a wurtzite-type lattice of bulk CdSe, yielding a $Cd_{33}Se_{33}$ nanocrystal of ~1.3−1.5 nm diameter (Scheme 1d). During geometry optimization, the surface reconstruction is significant, which is typical for such small semiconductor nanostructures.[86] Finally, both ligated and unligated clusters adopt a characteristic cage−core shape.[12,13,86] Such optimized structures have been extensively used in our previous work[12,13] and have been reported in a recent detailed DFT study.[86]

In addition to the unpassivated dot, two different capping ligands were chosen to simulate saturation of surface dangling bonds: methylamine (NH_2Me), and trimethyl phosphine oxide ($OPMe_3$). These are chemically reduced models approximating common surface-agents for CdSe QDs.[13] Following our previous studies,[13,25] partial ($9OPMe_3$ and $9NH_2Me$) and full ($21NH_2Me$) surface passivations were explored. The initial geometries (one unpassivated and three ligated clusters) have been optimized using the Gaussian 03 package,[87] utilizing the hybrid DFT functional B3LYP with a LANL2dz (Cd, Se atoms)/6-31G* (C, H, N, O, P atoms) basis set partitioning. The obtained optimized geometries are further used for calculations of 1PA spectra by linear-response formalism within the TD-DFT framework. For all studied systems, the first 150 excited states have been calculated. These simulations have been followed by calculations of 2PA spectra as detailed in refs 25, 26, and 64. An empirical line-broadening of 0.1 eV is used for simulations of both 1PA and 2PA. This parameter value has been extensively used for simulating molecular NLO responses and providing comparisons with experimental spectra.[26] Solvent effects are included

via the polarizable continuum model (PCM) of solvation as implemented in Gaussian code.[87] Acetonitrile (MeCN, ε = 35.688) is used as a solvent to highlight changes for 1PA and 2PA spectra compared to that for the isolated QD clusters.

Conflict of Interest: The authors declare no competing financial interest.

Acknowledgment. This work was supported in part by grants from the DARPA ZOE program (Grant No. W31P4Q-09-1-0012), the NSF PREM (Grant No. DMR-0934212), and the NSF (Grant No. CHE-1213047). Los Alamos National Laboratory is operated by Los Alamos National Security, LLC, for the National Nuclear Security Administration of the U.S. Department of Energy under Contract DE-AC52-06NA25396. We acknowledge support of the Center for Integrated Nanotechnology (CINT) and Center for Nonlinear Studies (CNLS). S.K. acknowledges financial support of the US Department of Energy (DOE) Early Career Research Grant DE-SC008446.

Supporting Information Available: Description of the synthesis of quantum dots, effective-mass calculations, measurements of molar absorptivities, quantum yields, and lifetimes, as well as measurements of transient absorption spectra and discussion of the core/shell quantum dots. This material is available free of charge *via* the Internet at http://pubs.acs.org.

REFERENCES AND NOTES

1. Alivisatos, A. P. Semiconductor Clusters, Nanocrystals, and Quantum Dots. *Science* **1996**, *271*, 933–937.
2. Chan, W. C. W.; Nie, S. M. Quantum Dots Bioconjugates for Ultrasensitive Nonisotopic Detection. *Science* **1998**, *281*, 2016–2018.
3. Bruchez, M., Jr.; Moronne, M.; Gin, P.; Weiss, S.; Alivisatos, A. P. Semiconductor Nanocrystals as Fluorescent Biological Labels. *Science* **1998**, *281*, 2013–2016.
4. Padilha, L. A.; Fu, J.; Hagan, D. J.; Van Stryland, E. W.; Cesar, C. L.; Barbosa, L. C.; Cruz, C. H. B.; Buso, D.; Martucci, A. Frequency Degenerate and Nondegenerate Two-Photon Absorption Spectra of Semiconductor Quantum Dots. *Phys. Rev. B* **2007**, *75*, 075325.
5. Padilha, L. A.; Fu, J.; Hagan, D. J.; Van Stryland, E. W.; Cesar, C. L.; Barbosa, L. C.; Cruz, C. H. B. Two-Photon Absorption in CdTe Quantum Dots. *Opt. Expr.* **2005**, *13*, 6460–6467.
6. Padilha, L. A.; Nootz, G.; Olszak, P. D.; Webster, S.; Hagan, D. J.; Van Stryland, E. W.; Levina, L.; Sukhovatkin, V.; Brzozowski, L.; Sargent, E. H. Optimization of Band Structure and Quantum-Size-Effect Tuning for Two-Photon Absorption Enhancement in Quantum Dots. *Nano Lett.* **2011**, *11*, 1227–1231.
7. Pu, S.-C.; Yang, M.-J.; Hsu, C.-C.; Lai, C.-W.; Hsieh, C.-C.; Lin, S. H.; Cheng, Y.-M.; Chou, P.-T. The Empirical Correlation between Size and Two-Photon Absorption Cross Section of CdSe and CdTe Quantum Dots. *Small* **2006**, *11*, 1308–1313.
8. Qu, Y.; Ji, W. Two-Photon Absorption of Quantum Dots in the Regime of Very Strong Confinement: Size and Wavelength Dependence. *J. Opt. Soc. Am. B* **2009**, *26*, 1897–1904.
9. Padilha, L. A.; Nootz, G.; Webster, S.; Hagan, D. J.; Van Stryland, E. W.; Levina, L.; Sukhovatkin, V.; Sargent, E. H. Two-Photon Absorption and Multi-exciton Generation in Lead Salt Quantum Dots. *Proc. SPIE* **2010**, *7600*, 760008.
10. Fedorov, A. V.; Baranov, A. V.; Inoue, K. Two-Photon Transitions in Systems with Semiconductor Quantum Dots. *Phys. Rev. B* **1996**, *54*, 8627–8732.
11. Efros, Al.L.; Rosen, M. Quantum Size Level Structure of Narrow-Gap Semiconductor Nanocrystals: Effect of Band Coupling. *Phys. Rev. B* **1998**, *58*, 7120–7135.
12. Kilina, S.; Velizhanin, K. A.; Ivanov, S.; Prezhdo, O. V.; Tretiak, S. Surface Ligands Increase Photoexcitation Relaxation Rates in CdSe Quantum Dots. *ACS Nano* **2012**, *6*, 6515–6524.
13. Kilina, S.; Ivanov, S.; Tretiak, S. Effect of Surface Ligands on Optical and Electronic Spectra of Semiconductor Nanoclusters. *J. Am. Chem. Soc.* **2009**, *131*, 7717–7726.
14. Neukirch, A. J.; Hyeon-Deuk, K.; Prezhdo, O. V. Time-Domain *ab Initio* Modeling of Excitation Dynamics in Quantum Dots. *Coord. Chem. Rev.* **2014**, *263*, 161–181.
15. Puzder, A.; Williamson, A. J.; Zaitseva, N.; Galli, G.; Manna, L.; Alivisatos, A. P. The Effect of Organic Ligand Binding on the Growth of CdSe Nanoparticles Probed by *ab Initio* Calculations. *Nano Lett.* **2004**, *4*, 2361–2365.
16. Nguyen, K. A.; Pachter, R. D.; Paul, N. Computational Prediction of Structures and Optical Excitations for Nanoscale Ultrasmall ZnS and CdSe Clusters. *J. Chem. Theory Comput.* **2013**, *9*, 3581–3596.
17. Casida, M. E. In *Recent Advances in Density-Functional Theory Methods*; Chong, D. A., Ed.; World Scientific: Singapore, 1995; Vol. 3.
18. Denk, W.; Strickler, J. H.; Webb, W. W. Two-Photon Laser Scanning Fluorescence Microscopy. *Science* **1990**, *248*, 73–76.
19. Zhou, W.; Kuebler, S. M.; Braun, K. L.; Yu, T.; Cammack, J. K.; Ober, C. K.; Perry, J. W. An Efficient Two-Photon-Generated Photoacid Applied to Positive-Tone 3D Microfabrication. *Science* **2002**, *296*, 1106–1109.
20. Kogej, T.; Beljonne, D.; Meyer, F.; Perry, J. W.; Marder, S. R.; Bredas, J. L. Mechanisms for Enhancement of Two-Photon Absorption in Donor−Acceptor Conjugated Chromophores. *Chem. Phys. Lett.* **1998**, *298*, 1–6.
21. Rebane, A.; Makarov, N. S.; Drobizhev, M.; Spangler, B.; Tarter, E. S.; Reeves, B. D.; Spangler, C. W.; Meng, F.; Suo, Z. Quantitative Prediction of Two-Photon Absorption Cross Section Based on Linear Spectroscopic Properties. *J. Phys. Chem. C* **2008**, *112*, 7997–8004.
22. Bosshard, C.; Spreiter, R.; Giinter, P.; Tykwinski, R. R.; Schreiber, M.; Diederich, F. Structure−Property Relationships in Nonlinear Optical Tetraethynylethenes. *Adv. Mater.* **1996**, *8*, 231–234.
23. Tykwinski, R. R.; Gubler, U.; Martin, R. E.; Diederich, F.; Bosshard, C.; Gu1nter, P. Structure−Property Relationships in Third-Order Nonlinear Optical Chromophores. *J. Phys. Chem. B* **1998**, *102*, 4451–4465.
24. Drobizhev, M. A.; Makarov, N. S.; Tillo, S. E.; Hughes, T.; Rebane, A. Two-Photon Absorption Properties of Fluorescent Proteins. *Nat. Methods* **2011**, *8*, 393–399.
25. Tretiak, S.; Chernyak, V. Resonant Nonlinear Polarizabilities in the Time-Dependent Density Functional (TDDFT) Theory. *J. Chem. Phys.* **2003**, *119*, 8809–8823.
26. Terenziani, F.; Katan, C.; Blanchard-Desce, M.; Badaeva, E.; Tretiak, S. Enhanced Two-Photon Absorption of Organic Chromophores: Theoretical and Experimental Assessments. *Adv. Mater.* **2008**, *20*, 1–38.
27. Day, P. N.; Nguyen, K. A.; Pachter, R. TDDF Study of One- and Two-Photon Absorption Properties: Donor−π-Acceptor Chromophores. *J. Phys. Chem. B* **2005**, *109*, 1803–1814.
28. Tretiak, S.; Chernyak, V.; Mukamel, S. Origin, Scaling, and Saturation of Second Order Polarizabilities in Donor/Acceptor Polyenes. *Chem. Phys. Lett.* **1998**, *287*, 75–82.
29. Marder, S. R.; Cheng, L.-T.; Tiemann, B. G.; Friedli, A. C.; Blanchard-Desce, M.; Perry, J. W.; Skindhøj, J. Large First Hyperpolarizabilities in Push−Pull Polyenes by Tuning of the Bond Length Alternation and Aromaticity. *Science* **1994**, *263*, 511–514.
30. Johnsen, M.; Paterson, M. J.; Arnbjerg, J.; Christiansen, O.; Nielsen, C. B.; Jørgensenb, M.; Ogilby, P. R. Effects of Conjugation Length and Resonance Enhancement on Two-Photon Absorption in Phenylene−Vinylene Oligomers. *Phys. Chem. Chem. Phys.* **2008**, *10*, 1177–1191.
31. Antonov, L.; Kamada, K.; Ohta, K.; Kamounah, F. S. A Systematic Femtosecond Study on the Two-Photon Absorbing D−π-A Molecules−π-Bridge Nitrogen Insertion and Strength of the Donor and Acceptor Groups. *Phys. Chem. Chem. Phys.* **2003**, *5*, 1193–1197.
32. Lin, T.-C.; He, G. S.; Prasad, P. N.; Tan, L.-S. Degenerate Nonlinear Absorption and Optical Power Limiting Properties of Asymmetrically Substituted Stilbenoid Chromophores. *J. Mater. Chem.* **2004**, *14*, 982–991.
33. Huang, Z.; Wang, X.; Li, B.; Lv, C.; Xu, J.; Jiang, W.; Tao, X.; Qian, S.; Chui, Y.; Yang, P. Two-Photon Absorption of

New Multibranched Chromophores Based on Bis-(diphenylamino)stilbene. *Opt. Mater.* **2007**, *29*, 1084–1090.
34. Collings, J. C.; Poon, S.-Y.; Droumaguet, C. L.; Charlot, M.; Katan, C.; Pålsson, L.-O.; Beeby, A.; Mosely, J. A.; Kaiser, H. M.; Kaufmann, D.; *et al.* The Synthesis and One- and Two-Photon Optical Properties of Dipolar, Quadrupolar and Octupolar Donor−Acceptor Molecules Containing Dimesitylboryl Groups. *Chem.—Eur. J.* **2009**, *15*, 198–208.
35. Laheld, U. E. H.; Einevoll, G. T. Excitons in CdSe Quantum Dots. *Phys. Rev. B* **1997**, *55*, 5184–5204.
36. Dolai, S.; Nimmala, P. R.; Mandal, M.; Muhoberac, B. B.; Dria, K.; Dass, A.; Sardar, R. Isolation of Bright Blue Light-Emitting CdSe Nanocrystals with 6.5 kDa Core in Gram Scale: High Photoluminescence Efficiency Controlled by Surface Ligand Chemistry. *Chem. Mater.* **2014**, *26*, 1278–1285.
37. Wang, Y.; Zhang, Y.; Wang, F.; Giblin, D. E.; Hoy, J.; Rohrs, H. W.; Loomis, R. A.; Buhro, W. E. The Magic-Size Nanocluster $(CdSe)_{34}$ as a Low-Temperature Nucleant for Cadmium Selenide Nanocrystals; Room-Temperature Growth of Crystalline Quantum Platelets. *Chem. Mater.* **2014**, *26*, 2233–2243.
38. Franceschetti, A.; Fu, H.; Wang, L. W.; Zunger, A. Many-Body Pseudopotential Theory of Excitons in InP and CdSe Quantum Dots. *Phys. Rev. B* **1999**, *60*, 1819–1829.
39. Franceschetti, A.; Luo, J. W.; An, J. M.; Zunger, A. Origin of One-Photon and Two-Photon Optical Transitions in PbSe Nanocrystals. *Phys. Rev. B* **2009**, *79*, 241311(R).
40. Rabani, E.; Baer, R. Distribution of Multiexciton Generation Rates in CdSe and InAs Nanocrystals. *Nano Lett.* **2008**, *8*, 4488–4492.
41. Ekimov, A. I.; Onushchenko, A. A. Quantum Size Effect in Three-Dimensional Microscopic Semiconductor Crystals. *JETP Lett.* **1981**, *34*, 345–349.
42. Rossetti, R.; Nakahara, S.; Brus, L. E. Quantum Size Effects in the Redox Potentials, Resonance Raman Spectra, and Electronic Spectra of CdS Crystallites in Aqueous Solution. *J. Chem. Phys.* **1983**, *79*, 1086–1088.
43. Klimov, V. I. Optical Nonlinearities and Ultrafast Carrier Dynamics in Semiconductor Nanocrystals. *J. Phys. Chem. B* **2000**, *104*, 6112–6123.
44. Baban, C.; Rusu, G. I. On the Structural and Optical Characteristics of CdSe Thin Films. *Appl. Surf. Sci.* **2003**, *211*, 6–12.
45. Chung, S.-J.; Zheng, S.; Odani, T.; Beverina, L.; Fu, J.; Padilha, L. A.; Biesso, A.; Hales, J. M.; Zhan, X.; Schmidt, K.; *et al.* Extended Squaraine Dyes with Large Two-Photon Absorption Cross-Sections. *J. Am. Chem. Soc.* **2006**, *128*, 14444–14445.
46. Van Stryland, E. W.; Woodall, M. A.; Vanherzeele, H.; Soileau, M. J. Energy Band-Gap Dependence of Two-Photon Absorption. *Opt. Lett.* **1985**, *10*, 490–492.
47. Ninomiya, S.; Adachi, S. Optical Properties of Cubic and Hexagonal CdSe. *J. Appl. Phys.* **1995**, *78*, 4681–4689.
48. Makarov, N. S.; Lin, Q.; Velizhanin, K.; Klimov, V. I. PbSe/CdSe Core−Shell Colloidal Quantum Dots with Enhanced Optical Nonlinearities and Dual-Band Infrared/Visible Emission. OSA Nonlinear Optics Conference, Kohala Coast, Hawaii, July 21−26, 2013.
49. Kasuya, A.; Sivamohan, R.; Barnakov, Y. A.; Dmitruk, I. M.; Nirasawa, T.; Romanyuk, V. R.; Kumar, V.; Mamykin, S. V.; Tohji, K.; Jeyadevan, B.; *et al.* Ultra-stable Nanoparticles of CdSe Revealed From Mass Spectrometry. *Nat. Mater.* **2004**, *3*, 99–102.
50. Wang, Y.; Liu, Y.-H.; Zhang, Y.; Wang, F.; Kowalski, P. J.; Rohrs, H. W.; Loomis, R. A.; Gross, M. L.; Buhro, W. E. Isolation of the Magic-Size CdSe Nanoclusters $[(CdSe)_{13}(n\text{-Octylamine})_{13}]$ and $[(CdSe)_{13}(\text{Oleylamine})_{13}]$. *Angew. Chem., Int. Ed.* **2012**, *51*, 6154–6157.
51. Fischer, S. A.; Crotty, A. M.; Kilina, S. V.; Ivanov, S. A.; Tretiak, S. Passivating Ligand and Solvent Contributions to the Electronic Properties of Semiconductor Nanocrystals. *Nanoscale* **2012**, *4*, 904–914.
52. Makarov, N.; Rebane, A.; Drobizhev, M.; Wolleb, H.; Spahni, H. Optimizing Two-Photon Absorption for Volumetric Optical Data Storage. *J. Opt. Soc. Am. B* **2007**, *24*, 1874–1885.
53. Goodson, T. G. Optical Excitations in Organic Dendrimers Investigated by Time-Resolved and Nonlinear Optical Spectroscopy. *Acc. Chem. Res.* **2005**, *38*, 99–107.
54. Varnavski, O.; Yan, X. Z.; Mongin, O.; Blanchard-Desce, M.; Goodson, T. Strongly Interacting Organic Conjugated Dendrimers with Enhanced Two-Photon Absorption. *J. Phys. Chem. C* **2007**, *111*, 149–162.
55. Yu, W. W.; Qu, L.; Guo, W.; Peng, X. Experimental Determination of the Extinction Coefficient of CdTe, CdSe, and CdS Nanocrystals. *Chem. Mater.* **2003**, *15*, 2854–2860.
56. Hales, J. M.; Cozzuol, M.; Screen, T. E. O.; Anderson, H. L.; Perry, J. W. Metalloporphyrin Polymer with Temporally Agile, Broadband Nonlinear Absorption for Optical Limiting in the Near Infrared. *Opt. Expr.* **2009**, *17*, 18478–18488.
57. Duncan, T. V.; Rubtsov, I. V.; Uyeda, H. T.; Therien, M. J. Highly Conjugated (Polypyridyl)metal-(porphinato)zinc(II) Compounds: Long-Lived, High Oscillator Strength, Excited-State Absorbers Having Exceptional Spectral Coverage of the Near-Infrared. *J. Am. Chem. Soc.* **2004**, *126*, 9474–9475.
58. Makarov, N. S.; Campo, J.; Hales, J. M.; Perry, J. W. Rapid, Broadband Two-Photon-Excited Fluorescence Spectroscopy and Its Application to Red-Emitting Secondary Reference Compounds. *Opt. Mater. Express* **2011**, *1*, 551–563.
59. Makarov, N. S.; Drobizhev, M.; Rebane, A. Two-Photon Absorption Standards in the 550−1600 nm Excitation Wavelength Range. *Opt. Express* **2008**, *16*, 4029–4047.
60. Haus, J. W.; Zhou, H. S.; Honma, I.; Komiyama, H. Quantum Confinement in Semiconductor Heterostructure Nanometer-Size Particles. *Phys. Rev. B* **1993**, *47*, 1359–1365.
61. Göppert-Mayer, M. Uber Elementarakte Mit Zwei Quantensprüngen. *Ann. Phys.* **1931**, *401*, 273–294.
62. Efros, Al.L.; Rosen, M. Quantum Size Level Structure of Narrow-Gap Semiconductor Nanocrystals: Effect of Band Coupling. *Phys. Rev. B* **1998**, *58*, 7120–7135.
63. Drobizhev, M.; Meng, F.; Rebane, A.; Stepanenko, Y.; Nickel, E.; Spangler, C. W. Strong Two-Photon Absorption in New Asymmetrically Substituted Porphyrins: Interference between Charge-Transfer and Intermediate-Resonance Pathways. *J. Phys. Chem. B* **2006**, *110*, 9802–9814.
64. Masunov, A. M.; Tretiak, S. Prediction of Two-Photon Absorption Properties for Organic Chromophores Using Time-Dependent Density-Functional Theory. *J. Phys. Chem. B* **2004**, *108*, 899–907.
65. Tretiak, S.; Chernyak, V.; Mukamel, S. Origin, Scaling, and Saturation of Second Order Polarizabilities in Donor/Acceptor Polyenes. *Chem. Phys. Lett.* **1998**, *287*, 75–82.
66. Bartholomew, G. P.; Rumi, M.; Pond, S. J. K.; Perry, J. W.; Tretiak, S.; Bazan, G. C. Two-Photon Absorption in Three-Dimensional Chromophores Based on [2.2]-Paracyclophane. *J. Am. Chem. Soc.* **2004**, *126*, 11529–11542.
67. Katan, C.; Tretiak, S.; Werts, M. H. V.; Bain, A. J.; Marsh, R. J.; Leonczek, N.; Nicolaou, N.; Badaeva, E.; Mongin, O.; Blanchard-Desce, M. Two-Photon Transitions in Quadrupolar and Branched Chromophores: Experiment and Theory. *J. Phys. Chem. B* **2007**, *111*, 9468–9483.
68. Pokrant, S.; Whaley, K. B. Tight-Binding Studies of Surface Effects on Electronic Structure of CdSe Nanocrystals: The Role of Organic Ligands, Surface Reconstruction, and Inorganic Capping Shells. *Eur. Phys. J. D* **1999**, *6*, 255–267.
69. Frenzel, J.; Joswig, J. O.; Sarkar, P.; Seifert, G.; Springborg, M. The Effects of Organisation, Embedding and Surfactants on the Properties of Cadmium Chalcogenide (CdS, CdSe and CdS/CdSe) Semiconductor Nanoparticles. *Eur. J. Inorg. Chem.* **2005**, *18*, 3585–3596.
70. Wang, L. W.; Zunger, A. Pseudopotential Calculations of Nanoscale CdSe Quantum Dots. *Phys. Rev. B* **1996**, *53*, 9579–9582.
71. Elward, J. M.; Chakraborty, A. Effect of Dot Size on Exciton Binding Energy and Electron-Hole Recombination Probability in CdSe Quantum Dots. *J. Chem. Theor. Comp.* **2013**, *9*, 4351–4359.
72. Reboredo, F. A.; Zunger, A. Surface-Passivation-Induced Optical Changes in Ge Quantum Dots. *Phys. Rev. B* **2011**, *63*, 235314.

73. Schapotschnikow, P.; Hommersom, B.; Vlugt, T. J. H. Adsorption and Binding of Ligands to CdSe Nanocrystals. *J. Phys. Chem. C* **2009**, *113*, 12690–12698.
74. Schapotschnikow, P.; van Huis, M. A.; Zandbergen, H. W.; Vanmaekelbergh, D.; Vlugt, T. J. H. Morphological Transformations and Fusion of PbSe Nanocrystals Studied Using Atomistic Simulations. *Nano Lett.* **2010**, *10*, 3966–3971.
75. Nguyen, K. A.; Day, P. N.; Pachter, R. Understanding Structural and Optical Properties of Nanoscale CdSe Magic-Size Quantum Dots: Insight from Computational Prediction. *J. Phys. Chem. C* **2010**, *114*, 16197–16209.
76. Zanjani, M. B.; Lukes, J. R. Size Dependent Elastic Moduli of CdSe Nanocrystal Superlattices Predicted from Atomistic and Coarse Grained Models. *J. Chem. Phys.* **2013**, *139*, 144702.
77. Albert, V. V.; Ivanov, S. A.; Tretiak, S.; Kilina, S. V. Electronic Structure of Ligated CdSe Clusters: Dependence on DFT Methodology. *J. Phys. Chem. C* **2011**, *115*, 15793–15800.
78. Fischer, S. A.; Crotty, A. M.; Kilina, S. V.; Ivanov, S. A.; Tretiak, S. Passivating Ligand and Solvent Contributions to the Electronic Properties of Semiconductor Nanocrystals. *Nanoscale* **2012**, *4*, 904–914.
79. Yang, P.; Tretiak, S.; Masunov, A. E.; Ivanov, S. Quantum Chemistry of the Minimal CdSe Clusters. *J. Chem. Phys.* **2008**, *129*, 074709.
80. Tohgha, U.; Deol, K. K.; Porter, A. G.; Bartko, S. G.; Choi, J. K.; Leonard, B. M.; Varga, K.; Kubelka, J.; Muller, G.; Balaz, M. Ligand Induced Circular Dichroism and Circularly Polarized Luminescence in CdSe Quantum Dots. *ACS Nano* **2013**, *7*, 11094–11102.
81. Lohne, M. P.; Hagen, G.; Hjorth-Jensen, M.; Kvaal, S.; Pederiva, F. *Ab Initio* Computation of the Energies of Circular Quantum Dots. *Phys. Rev. B* **2011**, *84*, 115302.
82. Khoshnegar, M.; Majedi, A. H. Single- and Few-Particle States in Core−Shell Nanowire Quantum Dots. *Phys. Rev. B* **2012**, *86*, 205318.
83. Isborn, C. M.; Kilina, S. V.; Li, X. S.; Prezhdo, O. V. Generation of Multiple Excitons in PbSe and CdSe Quantum Dots by Direct Photoexcitation: First-Principles Calculations on Small PbSe and CdSe Clusters. *J. Phys. Chem. C* **2008**, *112*, 18291–18294.
84. Ben, M. D.; Havenith, R. W. A.; Broer, R.; Stener, M. Density Functional Study on the Morphology and Photoabsorption of CdSe Nanoclusters. *J. Phys. Chem. C* **2011**, *115*, 16782–16796.
85. Azpiroz, J. M.; Ugalde, J. M.; Infante, I. Benchmark Assessment of Density Functional Methods on Group II−VI MX (M = Zn, Cd; X = S, Se, Te) Quantum Dots. *J. Chem. Theor. Comp.* **2014**, *10*, 76–89.
86. Nguyen, K. A.; Pachter, R.; Day, P. N. Computational Prediction of Structures and Optical Excitations for Nanoscale Ultrasmall ZnS and CdSe Clusters. *J. Chem. Theory Comput.* **2013**, *9*, 3581–3596.
87. Frisch, M.J.T.G.W.; Schlegel, H. B.; Scuseria, G. E.; Robb, M. A.; Cheeseman, J. R.; Montgomery, Jr.J. A.; Vreven, T.; Kudin, K. N.; Burant, J. C.; Millam, J. M.; *et al*. *Gaussian 09*, A.02; Gaussian Inc.: Wallingford CT, 2009.